EUROPEAN FUSION DEVELOPMENT AGREEMENT

EFDA–JET–PR(06)02

P. Buratti, B. Alper, S.. Annibaldi, A. Becoulet, P. Belo, J. Bucalossi, M. de Baar,
P. de Vries, D. Frigione, C. Gormezano, E. Joffrin, P. Smeulders
and JET EFDA contributors

Study of Slow n=1, m=1 Reconnection in JET Discharges with Low Central Magnetic Shear

Study of Slow n=1, m=1 Reconnection in JET Discharges with Low Central Magnetic Shear

P. Buratti[1], B. Alper[2], S.. Annibaldi[1], A. Becoulet[3], P. Belo[4], J. Bucalossi[3], M. de Baar[2], P. de Vries[2], D. Frigione[1], C. Gormezano[1], E. Joffrin[3], P. Smeulders[1] and JET EFDA contributors*

[1]EURATOM-ENEA Association, C.R. Frascati, CP 65, 00044 Frascati, Italy.
[2]*EURATOM/UKAEA Fusion Association, Culham Science Centre, Abingdon, OX14 3DB, UK*
[3]Association Euratom/CEA, Cadarache, France.
[4]Associação EURATOM/IST, Centro de Fusão Nuclear, 1049-001 Lisbon, Portugal,
** See annex of J. Pamela et al, "Overview of JET Results ",*
(Proc. 20th IAEA Fusion Energy Conference, Vilamoura, Portugal (2004)).

Preprint of Paper to be submitted for publication in
Plasma Physics and Controlled Fusion

ABSTRACT

Experiments designed for the attainment of the hybrid advanced mode of operation in JET revealed the existence of a new form of reconnecting modes with toroidal number $n = 1$ and poloidal number $m = 1$, which have the same radial localization as sawtooth precursors, but are characterized by small growth rate and low saturation amplitude. These modes develop in repetitive cycles with typical growth times of 100ms. Temperature perturbations are not in the form of sawteeth, in fact there is slow and mild erosion of the central temperature without any crash. Comparison with theory of $m = 1$ modes indicates that the slow growth observed in the hybrid regime is caused by the combined effect of low magnetic shear (a measure of the radial variation of field line inclination) and of peaked pressure in the plasma core.

1. INTRODUCTION

A new scenario of advanced operation, the so-called hybrid regime, has been recently developed in several tokamaks [1-6]. These experiments have demonstrated the possibility of operating at high plasma beta, with high confinement quality under reactor-relevant conditions [1]. The key distinguishing element of the hybrid scenario is the q profile (the safety factor q being the rate of change of toroidal flux with poloidal flux). In standard inductive tokamak operation there is a central region with $q<1$ where strong relaxation (sawtooth) instabilities take place. In contrast, sawteeth are either absent or very small in hybrid scenarios, which have a broad central region with low magnetic shear and $q\approx1$. An important issue for the validation of the hybrid scenario is stability of the $q\approx1$ region in the presence of fast particles and dominant electron heating. Such a regime has been recently investigated in experiments with Ion Cyclotron Resonance Heating (ICRH) at JET [3]. Internal MHD modes with toroidal number $n = 1$, which resemble resistive internal kinks (or sawtooth precursors) in their localization, but evolve very slowly and saturate at low amplitude, were identified in these experiments. Temperature perturbations by these modes are not in the form of sawtooth oscillations, but the amplitude of magnetic oscillations has the form of slow sawteeth with typical growth times of 100ms; for this reason, the observed modes have been indicated as "slow sawteeth" [3]; in the following the term sawteeth will be reserved for ordinary temperature profile relaxations, while slowly growing modes will be indicated as "reconnecting $n = 1$ modes". Besides practical aspects related to plasma performance (control of impurity accumulation on the hand and triggering of disruptive modes on the other hand), experiments in the hybrid scenario give the possibility of studying resistive internal kinks in conditions of very low magnetic shear; this is a valuable piece of information, since the dynamics of these modes and their relationship with sawtooth collapses is not fully understood at present. In this paper, experimental results on modes associated with the $q\approx1$ region will be presented and compared with theoretical estimates. The essential features of the hybrid regime with ICRH and its general MHD properties are presented in sec.2. The $n = 1$ modes are identified and compared with sawteeth relaxations in sect.3. Typical cycles of reconnecting $n = 1$ modes are analysed in detail in sect.4. Finally, experimental results are discussed and compared with theory in sect.5.

2. SCENARIO AND DIAGNOSTICS

The hybrid regime of operation was obtained in JET by applying a small amount of Lower Hybrid Current Drive (LHCD) during the current rise phase and by optimising the timing of the main heating power [2,3]. Experiments were mostly performed at B = 1.7T with Neutral Beam Injection (NBI) heating in order to achieve high beta and to perform similarity experiments [2]. A series of experiments aimed at establishing the hybrid regime in conditions of dominant electron heating was performed using ICRH at B=3.2T, with low hydrogen minority concentration (4-5%) for electron heating [3]. Total injected power was more than three times the L-H threshold and confinement was in H-mode, but activity of Edge Localized Modes (ELMs) remained of type III at very low level [3]. An example of such a discharge at plasma current I_p = 2.3MA and safety factor at the surface encircling 95% of magnetic flux q_{95} = 4.55 is shown in figure 1. The plasma shape is shown in figure 2. The normalized beta remained below 1.6 in these experiments due to power limitations; however the reduced amount of bootstrap current was partly compensated by LHCD. NBI also contributed to broadening the current profile, as shown by a decrease of internal inductance at the beginning of NBI heating.

The measurements of MHD modes are performed on JET using a set of fast magnetic pick-up coils distributed poloidally and toroidally inside the vacuum vessel. Toroidal mode numbers (n) of up to 64 can be determined from a set of coils distributed non-uniformly at the low-field side around the torus. Several sets of coils in poloidal planes determine the poloidal mode numbers (m) of the modes. The n number is well identified for each mode, while identification of the m number is affected by toroidal and shaping effects. Information on the radial structure of MHD modes is mainly obtained from profiles of temperature oscillation measured by electron cyclotron emission (ECE) at 48 radial positions and from soft X-ray cameras. A dashed line in figure 2 shows the ECE line of sight; profiles presented in the following sections are projected on the magnetic axis plane following the equilibrium flux surfaces. All the relevant diagnostic channels are recorded in selected time windows at a rate of 250kHz; in addition, some channels are recorded for longer periods at the same rate and a few channels are recorded at 2MHz in order to detect Alfvén waves.

2.1. OVERVIEW OF MHD ACTIVITIES IN THE HYBRID REGIME

One of the most attractive features of the hybrid regime is the low saturation level of MHD perturbations [6,7]. The main observed activities are intermittent m = 1, n = 1 fishbones and continuous tearing modes, typically n = 2, m = 3 and/or n = 3, m = 4 [2]. n = 1, m = 1 modes that differ from fishbones for having long duration and constant or increasing frequency are observed occasionally. Strong MHD is only observed at the beta limit in the form of large n = 1, m = 2 modes [4].

In hybrid plasmas with strong ICRH, fishbones become rare and acquire large frequency span (figure†3(a)), while cycles of long-lasting modes are the dominant n=1 activity; one cycle can be seen in figure†3(a) and four cycles in figure†3(b). The amplitude of these modes has the form a slow sawtooth during each cycle, as discussed in section†4. Tearing modes with n=2 are present in

most cases from the beginning of main heating; weaker modes with n up to 5 are observed occasionally. Two bands of Alfvén eigenmodes are observed, corresponding to toroidicity and ellipticity-induced gaps (see section 4.4 and [8]). All these feature are common to a series of hybrid discharges with a range of plasma currents $1.9 < I_p < 2.6$MA, corresponding to $5.5 > q_{95} > 3.8$.

3. IDENTIFICATION OF N=1 MODES

The spatial structure of $n = 1$ oscillations can be extracted from diagnostics sensitive to local temperature oscillations such as Electron Cyclotron Emission (ECE) or soft x-ray emission. In particular, frequency-selective coherence analysis between a reference magnetic signal and 48 ECE channels gives the profile of $n = 1$ temperature oscillations δT_e, while the ratio between δT_e and the time-average temperature gradient gives the flux-surface displacement. Figure 4(b) shows a typical δT_e profile. Temperature oscillations are localized within a distance of 0.25 m from the plasma center. The profile of temperature oscillations is of the resistive-internal-kink type, with phase difference between consecutive channels jumping by π (phase inversion) near the foot, as marked by an arrow in the figure. The maximum oscillation amplitude corresponds to a peak-to-peak displacement $\Delta = \delta T_e / |dT_e/dR| = 1.8$cm. Figure 4(a) gives the q-profile as measured by motional Stark effect (MSE) at the nearest available time. The q values in the central region are slightly above one, but, if the q-profile is lowered by 7% (within the errors of profile reconstruction), a $q = 1$ resonance appears at the foot of the temperature oscillation profile. Magnetic shear at this radius is $s_1 \approx 0.1$. The macroscopic effect of the n=1 mode on temperature profiles are shown in figure 4(c): Central electron temperature decreases by less than 5% during mode development, as shown in more detail in figure†4(d). The localisation of n=1 modes in the $q \approx 1$ region leads to identify the dominant poloidal number as m=1.

3.1 COMPARISON WITH FAST SAWTOOTH COLLAPSES

The mode numbers and profiles of temperature oscillations shown in figure 4 are similar to the ones of sawtooth precursors, but there are two striking differences. First, reconnecting $n = 1$ oscillations are long-lasting (200ms typically, see figure 3), while ordinary sawtooth precursors are much faster (<1ms typically); second, the effect of reconnecting modes is a mild erosion of temperature profiles (figures 4(c) and 5(a)), very different from the flattening produced by normal sawteeth (figure 5(b)). Discharges compared in figure 5 have same current, magnetic field and heating composition; the only difference is current profile evolution, which gives internal inductance $l_i = 0.8$ in case (a) and $l_i = 1.1$ in case (b).

4. AMPLITUDE AND FREQUENCY EVOLUTION OF RECONNECTING $N = 1$ MODES

A discharge free from the n=2 tearing mode was selected for a detailed study of n=1 modes evolution. The reason is that the presence of an n=2 mode at twice the frequency of the n=1 mode hampers the study of nonlinearly generated overtone harmonics. As shown in figure†6(d), in the selected discharge

(the same considered in figure 1) there are $n = 1$ and $n = 3$ modes. Figures 6(b) and (c) respectively show the amplitude of temperature and magnetic field oscillations associated with $n = 1$ modes, as obtained by rectifying signals after band-pass filtering between 4 and 8kHz. Both signals show that the cycles of $n = 1$ modes reach progressively larger amplitudes. The amplitude of magnetic signals tends to saturate in the first cycles (t<13s) and tends to grow exponentially in the following ones. This variation of $n = 1$ mode characteristics is associated with progressive peaking of the current density profile, as indicated by the increase of internal inductance (figure 6(a)), while heating conditions and density do not change (figure 1). The gross features of temperature oscillations agree with those of magnetic oscillations, although the details are different. This aspect will be examined in the following subsections, in which two typical examples of saturating and exponential cycles will be analysed in detail.

Figure 6(d) shows the spectrogram of a magnetic signal. Shortly after the beginning of main heating ($t = 8$s) there is a fishbone and the $n = 3$ mode appears. At $t = 10.4$s frequency (f_3) of the $n = 3$ mode splits and eventually remains around 21†kHz, with small variations associated either to notches in NBI power (at $t = 13$s) or to strong $n = 1$ cycles ($t > 14.7$s). Radial analysis, which is available after $t = 12$†s, gives $m = 4$ for the $n = 3$ mode, the mode being localized at $R = 3.3$m. where $q<1.5$. Frequency splitting is due to unlocking between this mode and another one with higher m. Cycles of $n = 1$ oscillations begin at $t = 9.5$s. During low-amplitude cycles, the $n = 1$ mode frequency (f_1) increases starting from 4 kHz and saturates at about 7kHz, while the frequency ramp disappears in stronger cycles after $t = 13$s. Interestingly, f_1 saturates at exactly $f_3/3$, and the excursion of f_1 during low-amplitude cycles equals the electron diamagnetic frequency $f_{*e} = T_{eV}/2\pi B r_1 L_p$, where r_1 is the average $q = 1$ radius and L_p is pressure scale length at q=1. Near the end of each cycle a weak $n = 2$ second harmonic component appears.

4.1 DETAILS OF A SATURATING CYCLE

The main features of saturating (low-amplitude) cycles of $n = 1$ reconnecting modes are frequency variation, weak amplitude and smooth evolution (no fast transients). As shown in figure 7(d,e), there are some bursts of low-frequency (4kHz) activity, after which the $n = 1$ mode starts at 4†kHz and evolves to 7kHz. The amplitude evolution of magnetic oscillations (figure 7(d)) increases linearly in time for 250ms, saturates for about 50†ms and then decays to a much lower level in about 10ms, the latter being the faster time-scale observed in saturating cycles. Central electron temperature (figure 7(a)) starts decreasing when oscillation amplitude is close to the saturation value and recovers when magnetic oscillations decay. Temperature oscillation profiles in the saturated stage are given in figure 4(b). At $t = 12.29$s, when magnetic oscillations decay, the amplitude of channels outside the phase inversion (i.e. π phase jump) radius drop to the noise level (figure 7(c)), while substantial amplitude remains in more central channels (figure 7(b)).

4.2 DETAILS OF AN EXPONENTIAL CYCLE

The exponential cycle shown in figure 8 starts at t = 14.04s after two very weak saturating cycles. The amplitude of magnetic oscillations grows exponentially with growth rate $\gamma = 11 s^{-1}$. Mode frequency is nearly constant. Temperature oscillation profiles evolve from tearing-like, with substantial oscillations outside the phase inversion radius, (figure 9(a)) to resistive-kink-like (figure 9(b,c)). Amplitude outside the phase inversion radius is larger than in the saturating case. The evolution of central channels is rather involved, with a temporary decrease accompanied by the development of a strong second harmonic (frequency doubling, see section 4.3) around t = 14.2s, followed by a rapid increase and by a tail during temperature recovery. Central soft x-ray channels have similar beahviour.

The perturbation of temperature profile is still within 5% (figure 10(a)), but a change on a fast time scale (of the order of 1ms) emerges at t = 14.25s, when the amplitude of magnetic oscillations drops. This rapid change is not visible in figure 8 because cross-coherence analysis has a time resolution of 8†ms, but duration can be inferred from magnetics raw data. During this transient there is fast mixing in an annular region surrounding the phase inversion radius, as evidenced by a huge increase of the rate of temperature variation (figure 10(d)). This event is accompanied by a burst of toroidal Alfvén eigenmodes that will be discussed in section 4.4.

4.3. FREQUENCY DOUBLING

Magnetic signals and temperature oscillations outside the phase inversion radius feature a second harmonic that increases together with the fundamental one and never overtakes it (figure 8(c,d)). MHD mode analysis shows that the second harmonic of magnetic signals has n = 2 toroidal mode number. In central ECE channels(figure 8 (b)) the second harmonic has completely different time evolution and can overtake the amplitude of the fundamental one. Figure 11 shows the amplitude of temperature oscillations in several channels for one of the strongest cycles; times at which second harmonic overtakes first harmonic show a clear progression towards the plasma center; the same figure shows for comparison first and second harmonics from magnetic signals. The appearance of a dominant second harmonic could be explained by a local modification of the magnetic structure by non-linear effects that generate a n = 2 component of the mode. Another possible explanation is the development of a temperature peak around the O-point of the magnetic island. The phenomenon of frequency doubling (meaning the presence of a dominant second harmonic, not necessarily complete suppression of the fundamental one) has been observed in the presence of m = 1, n = 1 magnetic islands in plasmas with strong electron heating [9] and has been explained by the formation of a local temperature peak inside the island, i.e. by a change of the $T(\psi)$ distribution inside the island, ψ being the helical flux coordinate. Simulations performed by the M1TEV code [9] assuming that cross-field transport inside the island is not faster than in the surrounding plasma, have shown that a temperature peak appears inside the island in about 100 ms, in agreement with experimental results. In this context the progression of crossing times shown in figure†11 would be justified by propagation of the island O-point towards the plasma center.

4.4. INTERACION WITH FAST PARTICLES

Hybrid discharges with strong ICRH feature a band of spectral lines between 150 and 220kHz and another one between 500 and 560kHz [8]. Since the Alfvén frequency $f_A = V_A/2\pi R$ = 520kHz and keeping Doppler shift into account, the first band results to be due to Toroidal AlfvÈn eigenmodes (TAE) localized in the $q \approx 1.5$ region (the TAE frequency being $f_{TAE} = f_A/2q$). The upper band is due to Ellipticity-induced Alfvén Eigenmodes (EAE) localized in the $q = 1$ region (the EAE frequency being $f_{EAE} = f_A/q$).

During the growth of the n=1 mode there is a progressive enhancement of EAE lines, while TAE lines stay at constant amplitude (figure 12(a,b)). After the drop of $n = 1$ magnetic oscillations TAE lines disappear and then recover at the same frequency on a time scale of 10ms; EAE lines weaken and recover on the same time-scale with slightly upshifted frequency. At the transition a burst in intensity is observed in the TAE region, indicating the rapid relocation of fast ions driving TAE modes. The duration of this transient is less than 1ms, as shown in the blow-up in figure 12. The maximum enhancement of oscillation amplitude in the TAE region (100-200kHz) is by a factor 20, while no significant enhancement is observed in the EAE region. The enhancement of TAE lines is strictly correlated with the presence of a fast rearrangement of the temperature profile, in fact both the fast temperature transient and the TAE burst are absent in weak $n = 1$ cycles.

DISCUSSION

Cycles of $n = 1$ modes observed in hybrid plasmas appear as an extremely slow and weak form of sawtooth relaxations. Time taken to reconnect magnetic flux across less than 10% of the $q = 1$ radius is typically longer than 100ms (see figure 7). We compared this time with the one calculated by Kadomtsev [10] for full reconnection inside the $q = 1$ radius, i.e. $\tau_K = \tau_A(\tau_\eta/s_1)^{1/2}$, where τ_h and τ_A are resistive diffusion time and Alfvén time respectively and s_1 is magnetic shear at the $q = 1$ radius. For plasma parameters appropriate to the case shown in figure 7 $\tau_\eta = 10.6$s and $\tau_A = 5.4 \times 10^{-7}$s; assuming $s_1 = 0.1$ as a typical low-shear value, we find $\tau_K = 7.6$ms. The Kadomtsev model only includes resistive reconnection and it usually overestimates the duration of sawtooth crashes, instead in our case we have that the experimental time for reconnection in a narrow layer is at least one order of magnitude longer than the one calculated for full reconnection.

In order to compare our results with more recent theories, we considered the growth rate $\gamma_{exp} = d(\ln \delta T_e)/dt$ evaluated from amplitude evolution of internal temperature oscillations. Excluding periods with frequency doubling, for which temperature oscillations are not representative of mode amplitude, γ_{exp} ranges from 10 to 50s^{-1}. According to linear theory [11], the relevant growth rate of the $n = 1$, $m = 1$ mode in the absence of diamagnetic effects is given by

$$\gamma_\rho = 0.88(\rho_s/r_1)^{4/7} \tau_\eta^{-1/7} \tau_A^{-6/7} s_1^{6/7} \qquad (1)$$

where ρ_S is the ion sound Larmor radius. Substituting actual values ρ_S = 7.4mm, r_1 = 220mm, equation (1) gives $\gamma_p = 3 \cdot 10^3$ s^{-1}, which is much larger than the experimental values. Diamagnetic effects can

stabilize the mode if the diamagnetic frequency ω_{*i} is sufficiently larger than γ_p. The criterion $3\gamma_p = \omega_{*i}$ [11] yields a critical shear (s_{crit}) below which the mode should be stable. Estimating the ion temperature (which is was not available) from the electron one we have $\omega_{*i} = 2.6 \cdot 10^4$ rad/s and then $s_{crit} = 0.36$. Since this critical shear is larger than typical s_1 values in hybrid discharges, experimental results in section 4.1 can be understood as a manifestation of diamagnetic weakening of the $m = 1$ mode. Also the observation, shown in figure 6, that progressive current profile peaking is accompanied by strengthening of reconnecting modes is consistent with this explanation, in fact magnetic shear tends to increase as current penetrates towards the plasma center.

On the other hand, sections 4.2 and 4.4 show that a sudden transition to fast reconnection can occur after a long period of slow mode growth. Time resolution of amplitude detection is not adequate to resolve the fast reconnection phase, however the duration of this phase (1ms typical) indicates that the growth rate suddenly increases by two orders of magnitude, a feature that hardly could be explained by any linear theory.

The simplified picture discussed above is based on layer effects in the semicollisional regime, which holds when ρ_S is the dominant length and the resistive width $\delta_\eta = r_1(\tau_A/\tau_\eta/s_1)^{1/3}$ is subdominant; both kinetic effects arising from fast particles [11] and non linear effects have been neglected. Fast-ion effects are not likely to play any important role, in fact both smooth evolution and full sawtooth crashes can occur under the same heating and plasma density conditions. Meanwhile non linear effects could play a role, in fact the plasma displacement (2cm typically) exceeds the layer width $\rho_S \approx 7$ mm. It is important to remark at this point that the applicability of current theories of $n = 1$, $m = 1$ modes to this experimental context is not guaranteed, in fact the basic orderings of linear theories could be inappropriate at the low observed growth rates; furthermore helical flux conservation, on which non-linear analytic theories are based, is likely to be violated on the experimentally observed long time scales.

Reconnecting $n = 1$ modes have been found in more than 75% of hybrid JET discharges with dominant electron heating. No deleterious effect of these modes, such as NTM triggering, has been observed, in fact all the observed NTMs appeared before the onset of $n = 1$ modes. There are two main practical questions to be answered by means of future experiments, first, can $n = 1$, $m = 1$ modes trigger the deleterious $n = 1$, $m = 2$ mode as β_N will be increased above the value ($\beta_N = 1.5$) reached in these experiments? Second, can $n = 1$, $m = 1$ modes be exploited for the control of central impurity and ash concentration?

ACKNOWLEDGMENTS

The authors acknowledge very useful discussions with F. Zonca. This work, supported by the Euratom Communities under the contract of Association between EURATOM/ENEA, was carried out within the framework the European Fusion Development Agreement. The views and opinions expressed herein do not necessarily reflect those of the European Commission.

REFERENCES

[1]. Sips A C C. et al 2005 *Plasma Phys. Control. Fusion* **47** A19

[2]. Joffrin E 2005 *Nucl. Fusion* **45** 626

[3]. Gormezano C et al 2004 *Plasma Phys. Control. Fusion* **46** B435

[4]. Wade M R at al 2005 *Nucl. Fusion* **45** 407

[5]. Sakamoto Y et al 2005 *Nucl. Fusion* **45** 574

[6]. Staebler A 2005 *Nucl. Fusion* **45** 617

[7]. Belo P et al 2004 *Proc. 31st EPS Conf. on Plasma Physics* (London 2004) P1-170

[8]. Buratti P et al 2005 *Proc 32nd EPS Conf. on Plasma Physics* (Tarragona 2005) O1-004

[9]. Porcelli F et al 1999 *Phys. Rev. Lett.* **82** 1458

[10]. Kadomtsev B B 1975 *Sov. J. Plasma Phys.* 1 89

[11]. Porcelli F, Boucher D and Rosenbluth M N 1996 *Plasma Phys. Control Fusion* **38** 2163

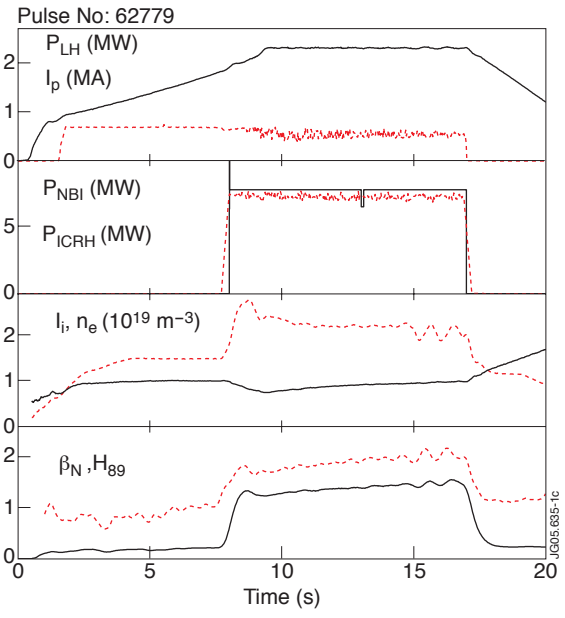

Figure 1: Main time-traces for a hybrid scenario with dominant electron heating. (a) Plasma current and LHCD power. (b) Main heating waveforms. (c) Internal inductance and line-average density. (d) Normalized beta and confinement enhancement factor.

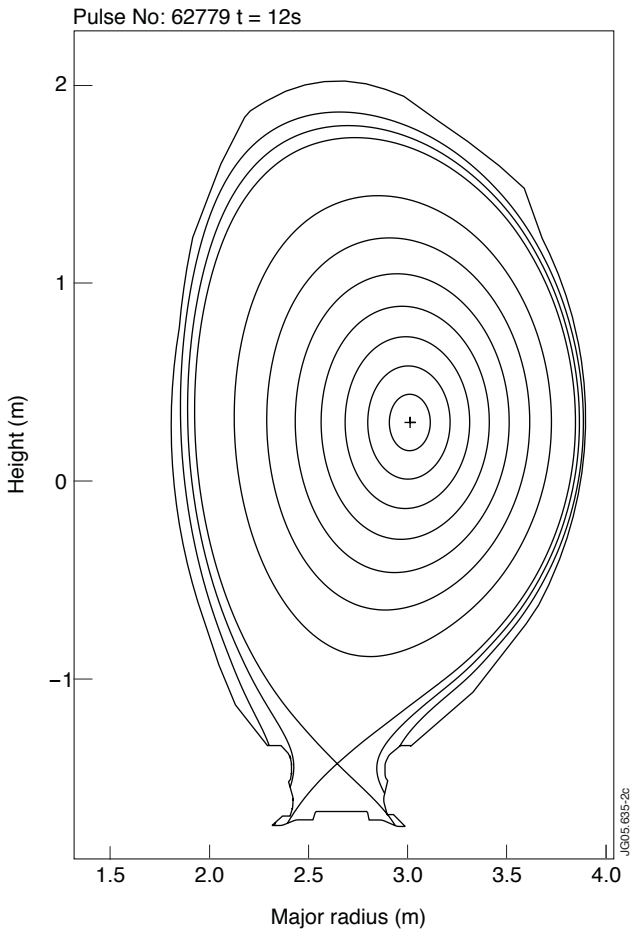

Figure 2: Magnetic flux contours for JET Pulse No:62779 at t=12s. Upper and lower triangularity are 0.16 and 0.25 respectively; elongation is 1.65. The thick contour indicates wall and divertor structures, the dashed line shows the ECE line of sight.

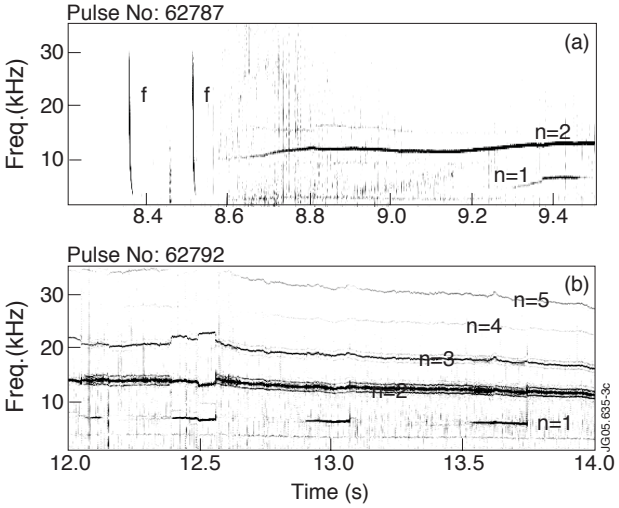

Figure 3. Typical spectrograms from a poloidal field pick-up coil. "f" indicates n=1 fishbones; other modes are labeled with their toroidal number. (a) JET Pulse No: 62787, with B=3.2T, I_p=2.3MA, 10MW ICRH, 8MW NBI starting at t=8s. (b) Pulse No: 62792, with B=3.2T, I_p=2.6MA, 10MW ICRH, 11MW NBI starting at t=9s.

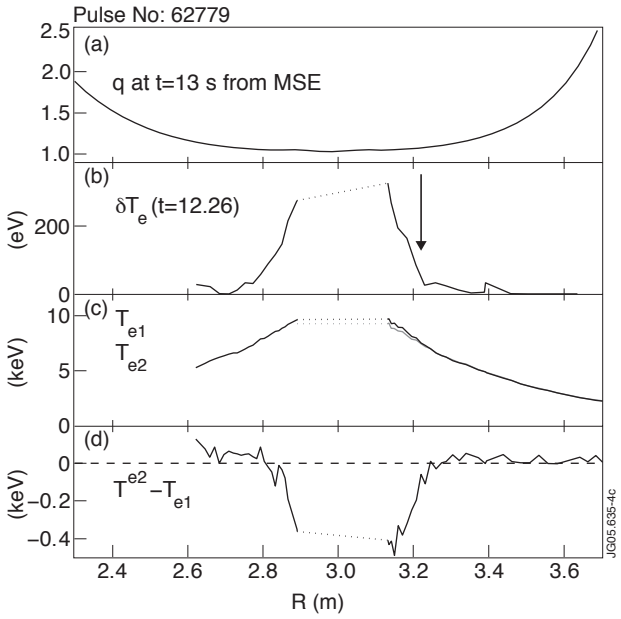

Figure 4. Radial analysis of n = 1 modes. (a) q-profile as measured by motional Stark effect. (b) Peak to peak amplitude of temperature oscillations from cross-coherence analysis of ECE and a reference magnetic signal; an arrow marks the position between two channels with p phase difference. (c) Electron temperature profiles at the beginning and at the end of the n = 1 cycle (t = 2.15 and 52.26s respectively). (d) Difference between profiles in (c). Profiles are projected on the equatorial plane; data along dotted segments are not available because the ECE line of sight is off-center.

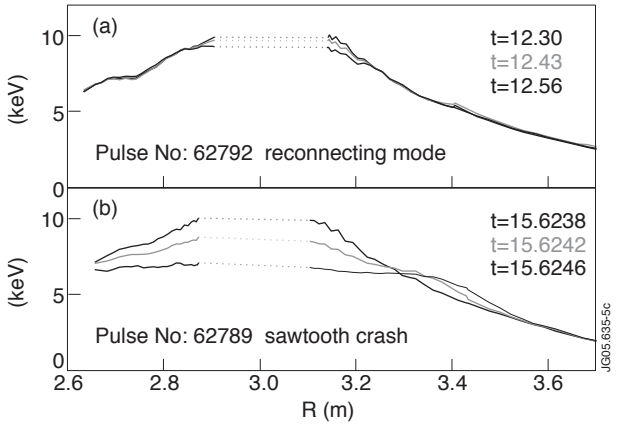

Figure 5: Temperature profile perturbation due to of n = 1 modes. (a) During a cycle of reconnecting mode. (b) In a normal sawtooth. Black lines represent profiles just before and at the top of temperature perturbation, gray lines at intermediate times. Note that time span is 260ms in (a) and 0.8†ms in (b). Both cases are at q_{95} = 3.8.

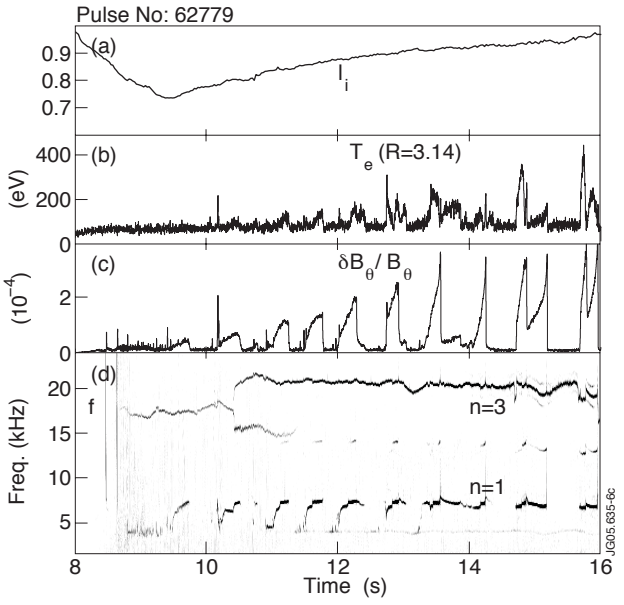

Figure 6: (a) Internal inductance. (b) Temperature oscillation amplitude in the n = 1 frequency band. (c) Magnetic field oscillation amplitude in the same band. (d) Spectrogram of magnetic field oscillations; "f" indicates an n = 1 fishbone, other modes are labeled with their toroidal number. Short-lived modes around 14kHz are n = 2 second harmonic components of n = 1 modes.

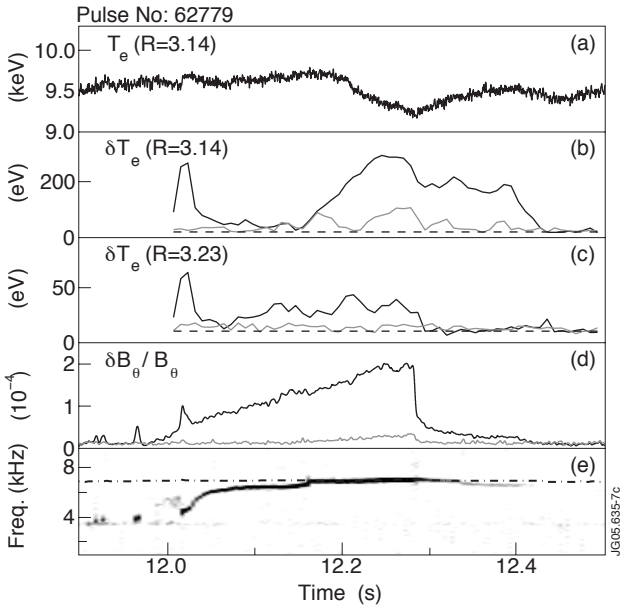

Figure 7: Evolution of a saturating n= 1 cycle. (a) Electron temperature near the plasma center. (b) Temperature oscillation amplitude near the plasma center from cross-coherence analysis at the n = 1 frequency (black) and at the second harmonic (gray); a dashed line shows the noise baseline. (c) Temperature oscillation amplitude near the phase-inversion radius. (d) Amplitude of magnetic oscillations. (e) Spectrogram of magnetic field oscillations; the dot-dashed line gives one third of the n = 3 mode frequency.

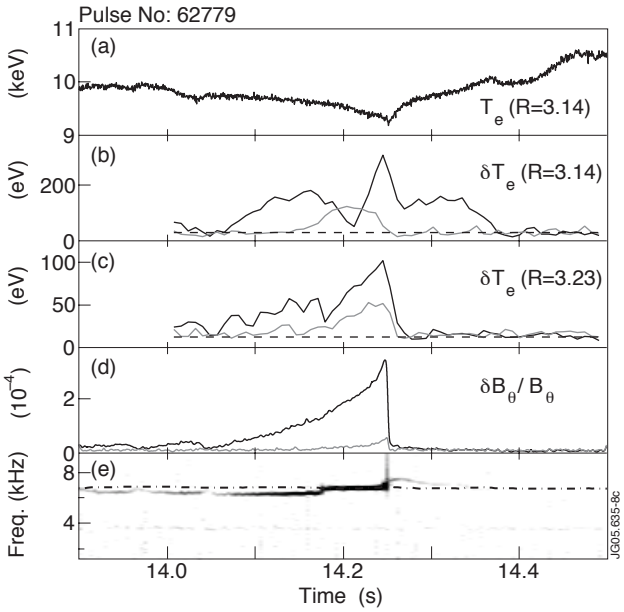

Figure 8: Evolution of an exponential n = 1 cycle. (a) Electron temperature near the plasma center. (b) Temperature oscillation amplitude near the plasma center from cross-coherence analysis at the n = 1 frequency (black) and at the second harmonic (gray); a dashed line shows the noise baseline. (c) Temperature oscillation amplitude near the phase-inversion radius. (d) Amplitude of magnetic oscillations. (e) Spectrogram of magnetic field oscillations; the dot-dashed line gives one third of the n = 3 mode frequency.

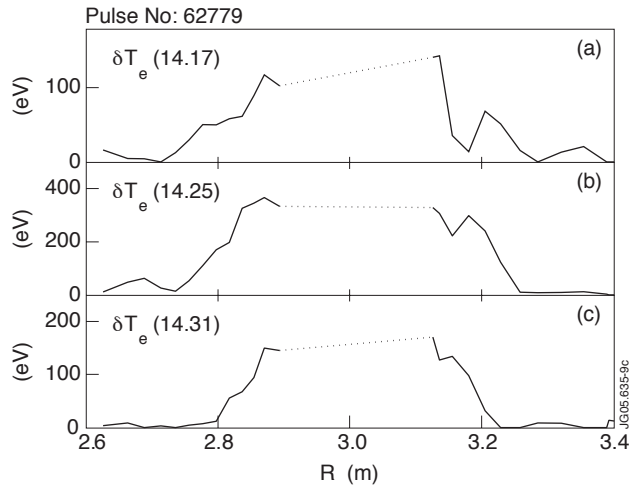

Figure 9. Radial profiles of n = 1 temperature oscillations from cross-coherence analysis during the cycle shown in figure 8. (a) Early stage. (b) Near top amplitude. (c) After the drop of magnetic oscillations. Arrows mark the position where cross-phase changes by π.

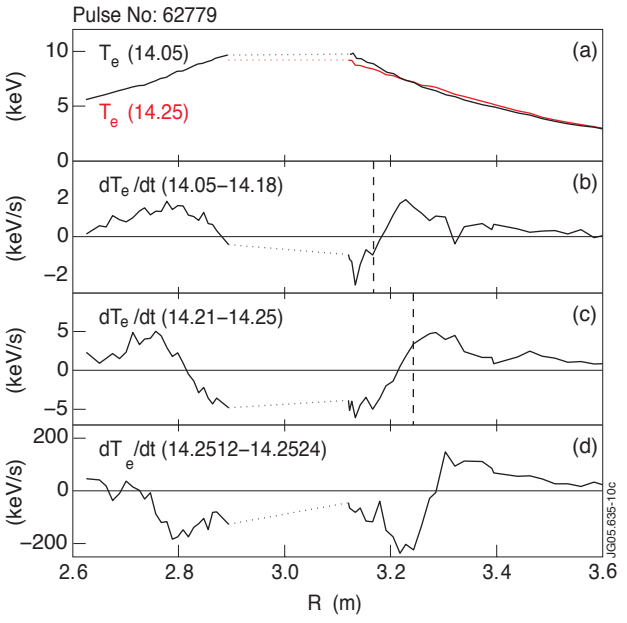

Figure 10. Evolution of temperature profiles during the cycle shown in figure 8. (a) Profiles before and at the extreme of temperature perturbation. (b) Rate of temperature variation in the early stage (see figure 9(a)). (c) Rate near top oscillation amplitude (see figure 9(b)). (d) Rate during the fast transient at the drop of magnetic oscillations. Vertical dashed lines mark the radii of phase inversion of temperature oscillations.

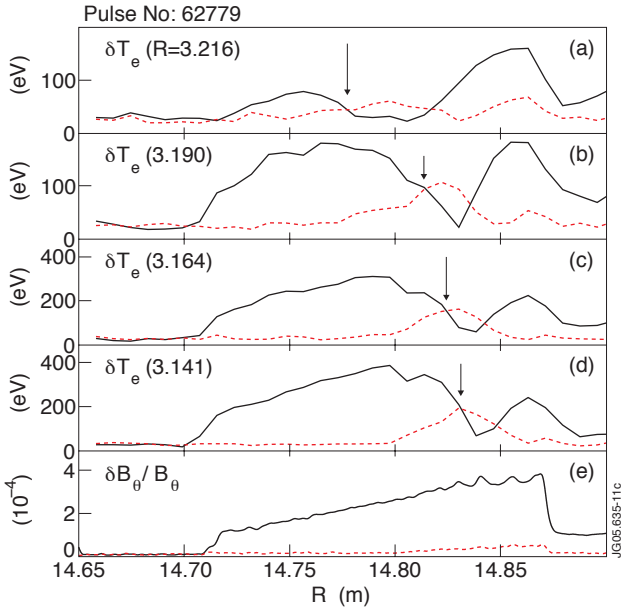

Figure 11: Amplitude of oscillations at the n = 1 frequency (black lines) and at the second harmonic (gray lines). (a)-(d) Temperature oscillations at progressively more internal positions; arrows mark crossing between fundamental and second harmonic. (e) Magnetic field oscillation amplitudes.

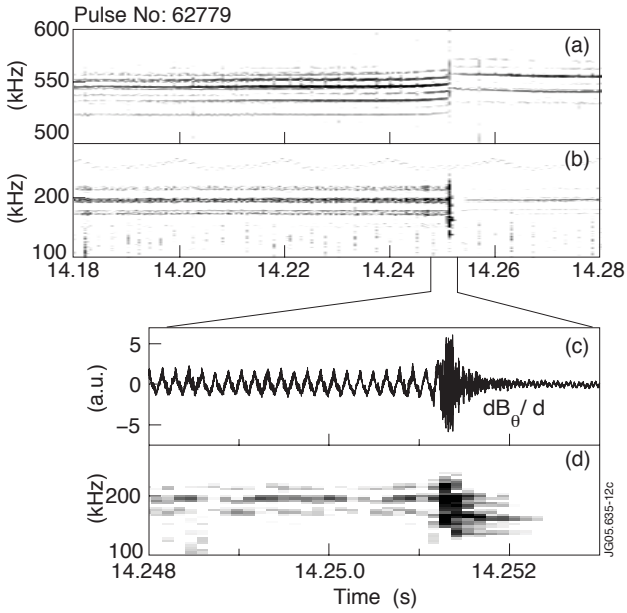

Figure 12. Evolution Alfvén eigenmodes in an exponential cycle. (a) Spectrogram of a magnetic signal in the EAE region. (b) Spectrogram in the TAE region. (c) Blow-up of the signal from a magnetic pick-up coil. Relatively slow oscillations at t<14.251s are due to the n = 1 mode. (d) High-time-resolution spectrogram of the magnetic signal in the TAE band. The burst of magnetic activity at the fast temperature transient is entirely due to strong enhancement of TAE lines.